RSC Advances

ROYAL SOCIETY OF CHEMISTRY

www.rsc.org/advances

Graphical abstract

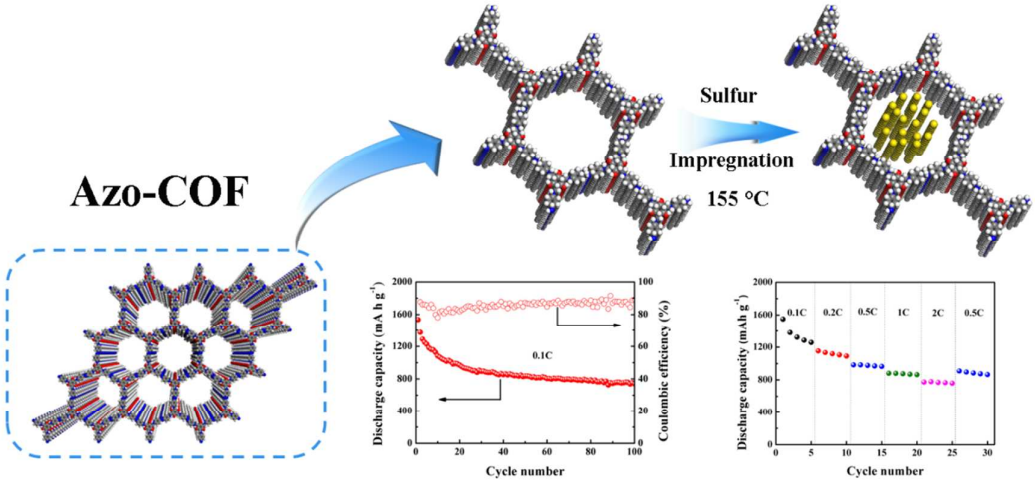

A novel mesoporous covalent organic frame with regular pore distribution was well designed for lithium-sulfur batteries.

Journal Name

ARTICLE

Sulfur impregnated in a mesoporous covalent organic framework for high performance lithium-sulfur batteries†

Received 0

1. Xiaofei Yang [a, c‡], Bin Dong [b‡], Hongzhang Zhang [a], Rile Ge [b], Yanan Gao *[b], Huamin Zhang *[a, d]

Received 00th January 20xx,
Accepted 00th January 20xx

DOI: 10.1039/x0xx00000x

www.rsc.org/

Undesirable cycling performance has been considered as the main bottleneck that hindered the practical application of lithium-sulfur (Li-S) batteries, which mainly results from soluble polysulfides shuttling between the anode and the cathode (so-called shuttle effect). To solve this problem effectively, a covalent organic framework (COF) named Azo-COF with a regular pore distribution at 2.6 nm was prepared as the host for sulfur. Such small mesopores can not only confine the sulfur well in the nanopores but also supply the Li^+ with one-dimension (1D) transmission channels. Benefit from this concept, even without $LiNO_3$ as additive, the Li-S batteries assembly with S/Azo-COF cathode presented a high stable capacity of 741 mA h g^{-1} after 100 cycles while delivered a high initial discharge capacity of nearly 1536 mA h g^{-1} at 0.1 C (1 C = 1672 mA g^{-1}). Additionally, when the capacity rate (C-rate) increased to 2 C, a high discharge capacity of 770 mA h g^{-1} can be still achieved after 20 cycles, proving the excellent C-rate performance.

Introduction

The widespread use of portable electronics and the desire for utilizing such renewable resources as solar, wind and tidal effectively have created great opportunities as well as challenges for the development of next-generation energy storage systems. State-of-the-art rechargeable batteries based on intercalation lithium, only present low typical capacity less than 250 mA h g^{-1} by using lithium transition metal oxides as cathode material,[1] which can not meet the increasing demand of power-intensive applications, including long-range electrical vehicles and stationary energy storage.[2] Hence, searching for a new cathode material with higher capacity and energy density as a replacement is of great concern. Recently, lithium-sulfur (Li-S) batteries have been proved to possess the potential to offer a superior theoretical specific capacity of 1675 mA h g^{-1} and energy density of 2500 Wh kg^{-1} on the basis of active sulfur, which is 3-5 times the magnitude of traditional Li ion batteries.[3, 4] In addition, the active sulfur, one of the most abundant elements in the earth's crust, is also cut-price and environmental friendly, co-making Li-S batteries a promising choice to replace Li ion batteries in next-generation storage systems with high energy density.[5, 6]

However, the Li-S batteries are still far from conquering the marketplace mainly due, at least in part, to their own drawbacks. Firstly, the specific capacity output of Li-S batteries is limited by poor utilization of active material caused by insulation nature of sulfur and lithium sulfide (Li_2S).[6-8] Moreover, a volumetric expansion of 80% was accompanied by lithiation of sulfur during discharge, which will give rise to mechanical damage of cathode materials.[9, 10] The last and most formidable problem is, namely, shuttle effect, which arises from soluble polysulfides (PS) shuttle between the cathode and the anode during cycling.[3, 11] All of issues mentioned above co-caused low capacity, low coulombic efficiency and fast capacity fading.

To tackle those problems, various nanostructural materials, aiming to embed sulfur species into the micro- or mesopores of the hosts such as amorphous carbon,[3, 6, 12-15] carbon nanotube,[7, 10, 16] carbon fibres,[17-20] graphene,[21-25] conducting polymers,[26-29] and metal oxides,[30, 31] have been reported. Unfortunately, in order to realize regular and suitable porous structures, such templates with accurate sizes as well as inconvenient and multistep synthesis procedures are evitable.[10, 19] COF, a member of porous materials' family, with regular pore distribution via strong chemical bond among the organic molecules, has shown the potential to be developed as sulfur container.[32, 33] For instance, Guo et al,[32] have confirmed that porous aromatic framework (PAF) could impede the PS diffusion effectively with a well defined pore distribution at 1.6 nm. 83% capacity content has been achieved after 50 cycles for the Li-S battery assembly with S/PAF cathode, showing excellent cycling stability. Despite its towering cycling performance, the C-rate performance has been greatly limited by low rate of Li^+

[a] Division of Energy Storage, Dalian Institute of Chemical Physics, Chinese Academy of Sciences, 457 Zhongshan Road, Dalian 116023, China; E-mail: zhanghz@dicp.ac.cn; Fax: +86-411-84665057; Tel.: +86-411-84379669
[b] Dalian Institute of Chemical Physics, Chinese Academy of Sciences, 457 Zhongshan Road, Dalian 116023, China; E-mail: ygao@dicp.ac.cn; Fax: +86-411-84379992; Tel.: +86-411-84379992
[c] University of Chinese Academy of Sciences, Beijing 100039, China
[d] *Collaborative Innovation Center of Chemistry for Energy Materials (iChEM), Dalian 116023 (P.R. China)*

† Electronic Supplementary Information (ESI) available: [details of any supplementary information available should be included here]. See DOI: 10.1039/x0xx00000x

transportation through such micropores. For example, when the C-rate increased to 2 C, only a low capacity of 334 mA h g^{-1} was maintained. The situation became worse, when the pores of this kind of hosts decreased to smaller size.[33] Hence, how to increase the C-rate performance of this kind of hosts has become the major problem need to be solved.

On this regard, the Azo-COF with larger 1D Li^+ transportation channel of 2.6 nm was prepared and studied for Li-S batteries application. As is well known, the channel with large scale can facilitate the Li^+ transport, which is helpful in enhancing the C-rate performance. As a result, such excellent Li-S battery performance as high active sulfur utilization, good cycling stability and C-rate capability was successfully achieved. In addition, the material preparation mechanism and the structure–performance relationship between the prepared Azo-COF and Li-S batteries were also studied in detail.

Experimental section

Preparation of S/Azo-COF composite

A pyrex tube (30 mL) was charged with Tp (63 mg, 0.3 mmol), Azo-diamine (94.5 mg, 0.45 mmol), and 3 mL of 1,4-dioxane. This mixture was sonicated for 10 min in order to get a homogeneous dispersion. The tube was then flash-frozen at 77 K (liquid N_2 bath) and degassed by three freeze-pump-thaw cycles. The tube was sealed off with a flame and then heated at 120 °C for 3 days. A dark-red precipitate was collected by filtration, washed with 1,4-dioxane and acetone for three times, and dried at 80 °C under vacuum for 12 h, the dark-red power named as Azo-COF of 125 mg was obtained (88 % yield).

The S/Azo-COF composite was prepared with a traditional method according to a previous report.[16] Typically, 0.3 g Azo-COF and 0.2 g commercial sulfur (Aldrich) were uniformly mixed. After that, the obtained mixture was put into a ceramic boat and heated at 155 °C for 20 h under Ar atmosphere. The obtained product was named as S/Azo-COF.

Materials Characterization

Field emission scanning electron microscopy (SEM) observations were performed on a Hitachi S-4800 microscope operated at an accelerating voltage of 10.0 kV. Tecnai G2TF20 scanning transmission electron microscope (STEM) equipped with Energy Dispersive X-Ray Spectroscopy (EDX) was used to evaluate the elements (carbon and sulfur) distribution. The nitrogen adsorption and desorption isotherms were measured at 77 K using a Quantachrome Quadrasorb SI system. Pore size distribution was calculated by applying nonlocal density functional theory (NLDFT) to the N_2 adsorption isotherm. Panalytical X'pert Pro Multipurpose Diffractometer was used to collect the powder X-ray diffraction data. The samples were mounted on a zero background sample holder measured using Cu Kα radiation (λ=0.154 nm, step size=0.017°). The thermal behavior was evaluated using a thermogravimetric analysis (TGA) instrument (STA PT1600 Linseis) under a nitrogen atmosphere with a heating rate of 10 °C min^{-1}.

Electrochemical Measurements

The electrochemical performance of the electrodes was carried out with CR2016 coin cells, which were fabricated in an Ar-filled glove box. The cathodes were prepared by casting a well-dispersed slurry of 60 wt.% active materials (S/Azo-COF), 30 wt.% conductive carbon (KB600), and 10 wt.% polyvinylidene fluoride (PVDF) in 1-methyl-2-pyrrolidinone (NMP) onto aluminium foil and then dried at 60 °C for 12 hours under vacuum. The average active sulfur loading is about 0.6~0.8 mg cm^{-2}, calculated on the basis of geometrical area of electrodes. The cathode and the anode (lithium foil) were separated by a celgard 2325 membrane doping with 1 M bis(trifluoromethylsulfonyl)imide (LiTFSI)–1, 2-dimethoxymethane (DME)/1, 3-dioxolane (DOL) (1:1 v/v) without $LiNO_3$ as additive.

The cyclic voltammetry (CV) was measured with CHI 611e electrochemical workstation (Shanghai Chenhua Corp.) with a scan rate of 0.1 mV s^{-1}. The charge-discharge test was carried out using a LAND CT-2001A system at room temperature. It should mentioned that the specific capacities and the voltage mentioned in this article were calculated on the basis of sulfur and respected to Li^+/Li (vs. Li^+/Li), respectively.

Results and discussion

The Azo-COF was synthesized using the Schiff base reaction between triformylphloroglucinol and 4,4'-azodianiline according to the literature,[34] as illustrated in Scheme 1. The morphology of Azo-COF and S/Azo-COF was observed through SEM (Fig. 1a-b). Even Azo-COF exhibits severe aggregation, individual particles with size less than 100 nm can be still observed. Compared to the initial Azo-COF, S/Azo-COF presents 2D laminated structure after sulfur impregnation, owing to mechanical effect during mixing process. Moreover, no obvious sulfur particles can be seen outside of Azo-COF, indicating that most sulfur was wrapped well within Azo-COF. The STEM image, EDX and corresponding element mapping were shown in Fig. 1c-e. As observed, both the EDX and element mapping shows that the S/Azo-COF composite contains four elements. Among them, the elements of C, N, O comes from the skeleton of Azo-COF and the element of S can be attributed to the sulfur impregnation. In addition, the similar shape and area of all of elements' mapping further demonstrated that the sulfur was well dispersed in the pores of Azo-COF.

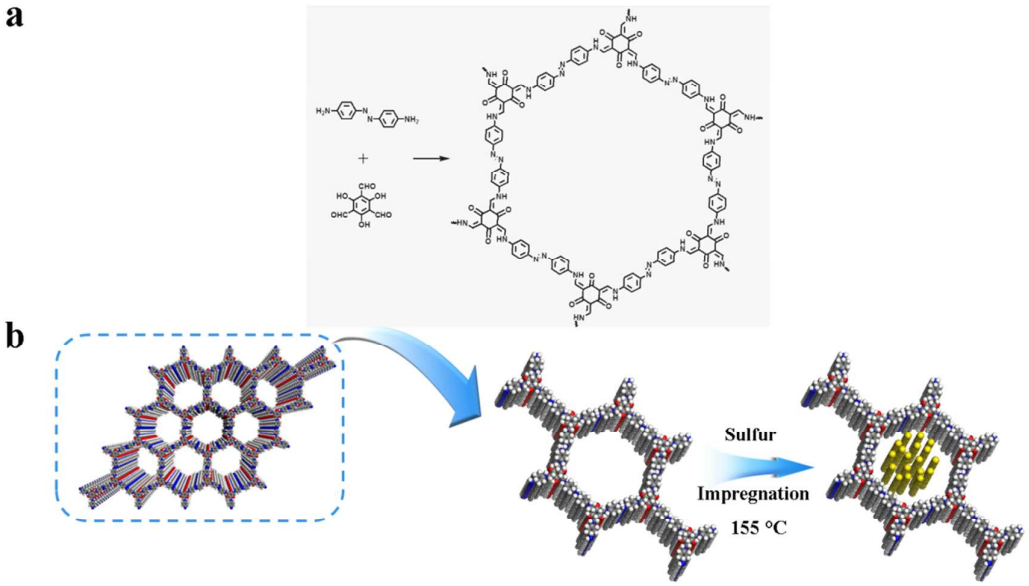

Scheme 1 Schematic illustration of the preparation of Azo-COF and S/Azo-COF composites.

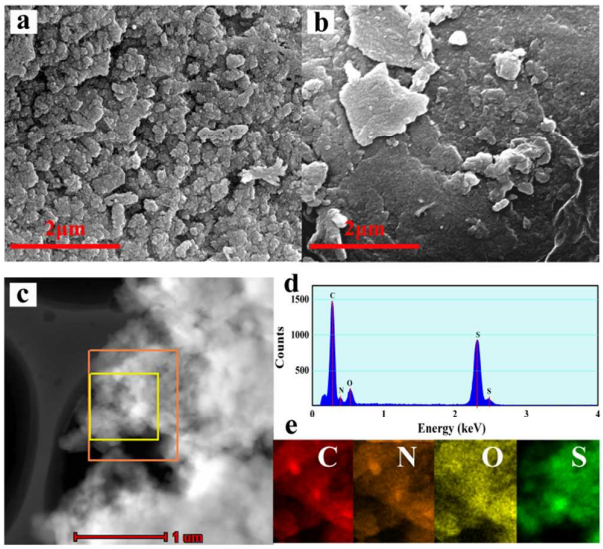

Fig. 1 SEM images of: (a) Azo-COF and (b) S/Azo-COF. (c) STEM image and (d) EDX of Azo-COF. (e) elemental mapping of C, N, O and S.

As shown in Fig. 2, the Brunauer-Emmett-Teller (BET) method was used to investigate the definite quantitative porous structures of Azo-COF and S/Azo-COF. An isotherm curve with strong absorption at both low relative pressure of 0~0.2 and high one larger than 0.9 can be observed from the N_2 adsorption—desorption isotherm of Azo-COF. It can be seen from Fig. 2b that only a sharp peak appeared at 2.6 nm for the sample of Azo-COF on the basis of Density Functional Theory (DFT) method. The regular pore distribution can be mainly owed to the orderly accumulation among the organic molecules via strong chemical force. Additionally, such small mesopores can not only suppress the diffusion of PS but also facilitate Li^+ transportation. That is to say, both the cycling performance and C-rate performance can be improved by using Azo-COF as the sulfur host. Owing to the abundant small mesopores at 2.6 nm, Azo-COF demonstrated a large surface area of 1150 $m^2 g^{-1}$ and a total pore volume of 0.90 $cm^3 g^{-1}$ (Table 1), which has been testified to be suitable for Li-S batteries application. After sulfur impregnation, the surface area and pore volume of the obtained S/Azo-COF composite decreased sharply to 56 $m^2 g^{-1}$ and 0.06 $cm^3 g^{-1}$, respectively. The sharp decrease of specific surface area and pore volume further revealed that most sulfur was impregnated in the small mesopores of the Azo-COF host, which is coincided well with the results of SEM and element mapping.

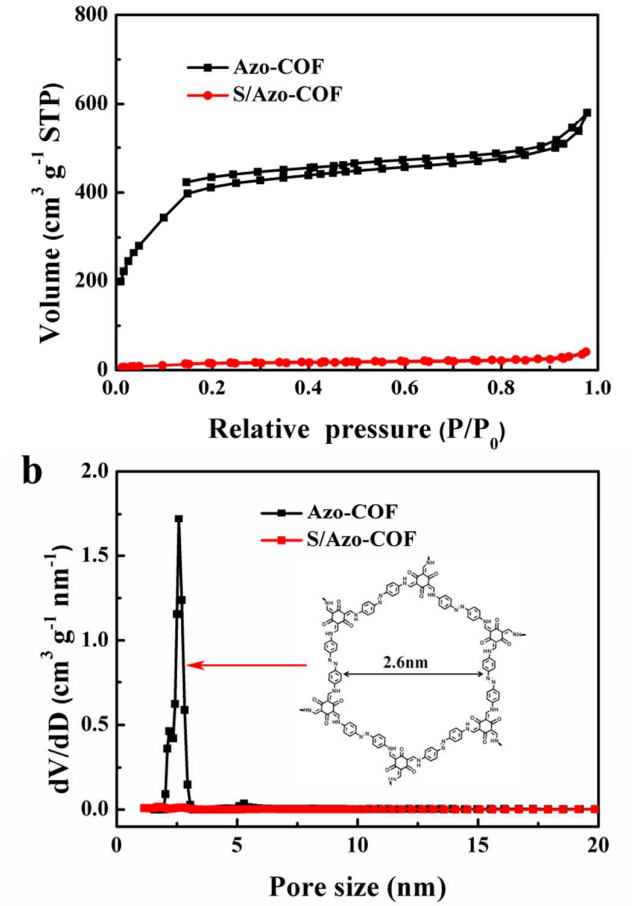

Fig. 2 (a) Nitrogen adsorption—desorption isotherms and (b) pore size distribution curves of Azo-COF and S/Azo-COF composites.

Table 1. Physical characteristics of Azo-COF and S/Azo-COF composites.

Sample	BET surface area (m^2 g^{-1})	Pore volume (cm^3 g^{-1})
Azo-COF	1150	0.90
S/Azo-COF	56	0.06

In order to further understand the formation of sulfur in Azo-COF after undergoing a heat treatment at 155°C, the crystal property of both sulfur and S/Azo-COF was characterized via X-ray diffraction (XRD), as shown in Fig. 3. For sulfur, characteristic pattern with intense peaks appeared between 10° and 40° accords to the orthorhombic structure of sulfur, which is the most stable model under natural conditions. After sulfur impregnated into Azo-COF, all of sharp peaks of crystalline sulfur disappeared and only two broad peaks located around 15° and 27° belong to Azo-COF exhibited (Fig S1), indicating that most sulfur is highly dispersed in the Azo-COF's pores.[6, 35]

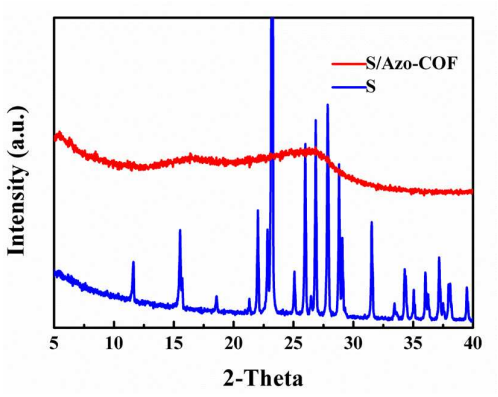

Fig. 3 XRD patterns of orthorhombic S and S/Azo-COF composite.

The thermal stability of Azo-COF and S/Azo-COF composite was characterized via TGA test. As shown in Fig. 4, for Azo-COF, when temperature increased to nearly 400 °C, a weight loss can be observed, suggesting that the Azo-COF is stable during sulfur impregnation procedure at 155°C. For S/Azo-COF, a new weight loss of nearly 39 wt% presented between 220 °C and 450 °C, which corresponds to the evaporation of sulfur in the composite materials. However, pure sulfur started to vapor at 200 °C and quickly vanished below 350 °C(Fig. S2). This output indicated that sulfur can be remained in the pores of the host stably,[36] which is in accordance with the XRD analysis. In other words, the sulfur species are more difficult to escape from the Azo-COF host, which is preferred in the Li-S batteries cycling process.

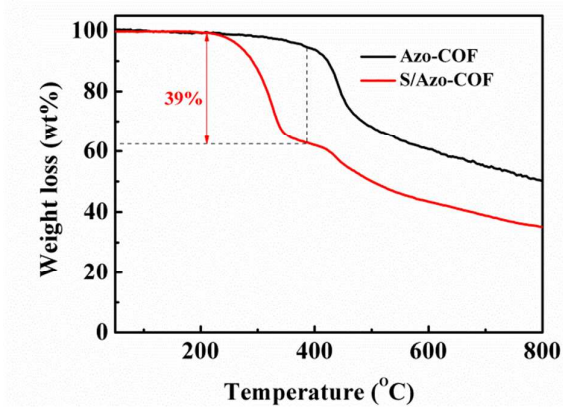

Fig. 4 TGA curves of the Azo-COF and S/Azo-COF composite.

Fig. 5 shows a typical CV curve with two reduction peaks and one oxidation peak of the S/Azo-COF composite, in which the two reduction peaks at about 2.3 V and 2.0 V can be ascribed to sulfur that was reduced to higher-order lithium PS (Li_2S_n, n≥4) and further reduced to lower-order lithium PS (Li_2S_n, n<4) respectively.[37, 38] The oxidation peak at about 2.4 V exhibits the reverse reaction from Li_2S and/or Li_2S_2 to final oxidation products of sulfur. Similar to the previous reports,[39-41] the reduction peak at 2.0 V exhibits the trend

to the higher potential, owing to redistribution of sulfur species that can enhance the electrochemical reversibility. Meanwhile, no obvious decay can be seen from both the oxidation and reduction peaks' intensity, further demonstrating that the sulfur species can be confined well in the Azo-COF host.

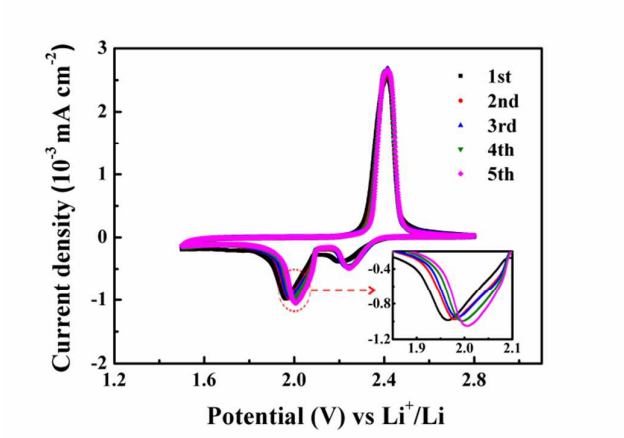

Fig. 5 CV curves of Azo-COF electrodes at a scanning rate of 0.1 mV s^{-1} ranging from 1.5 to 2.8 V with 5 cycles;

In order to clarify the advantage of Azo-COF structure, the cycling performance of S/Azo-COF cathode was investigated at a C-rate of 0.1 C (1 C = 1672 mA h g^{-1}) between 1.5 and 2.8 V. As shown in Fig. 6a, a high original discharge capacity of 1536 mA h g^{-1}, 91.9% of theoretical capacity, was exhibited for the cell assembly with S/Azo-COF cathode, indicating that poor electronic conductivity of Azo-COF has no negative influence upon the specific capacity output. Similar to the previous reports,[23, 39, 41-44] the discharge capacity decreases sharply in the first few cycles, which attributes to irreversible dissolution of PS. After that, a relatively stable capacity of 1082 mA h g^{-1} was achieved after 10 conditioning cycles. Within the next 90 cycles, a high discharge capacity of 741 mA h g^{-1}, corresponding to nearly 70% capacity retention, was remained even in a typical electrolyte (1M LiTFSI in DME/DOL (1:1 v/v)) without $LiNO_3$ as additive, which was calculated from the tenth cycle. What's more, the galvanostatic charge–discharge curves with two obvious discharge plateaus around 2.3 V and 2.1 V at a C-rate of 0.1 C for the S/Azo-COF cathode were shown in Fig. 6b. In general, the two plateaus can be ascribed to a two-step discharge process from sulfur to high-order lithium PS and further lithiation to Li_2S/Li_2S_2.[45] The low voltage drop and small capacity loss after ten cycles demonstrate that PS can be confined well in the Azo-COF host. a strong ability of FLHPC to inhibit the PS diffusion. In addition, when the C-rate increased to 1C, a high initial discharge capacity of 1044 mA h g^{-1} was still presented and a capacity of 602 mA h g^{-1} was maintained (Fig. 6c). Such good cycling performance of S/Azo-COF electrode can be mainly attributed to the relatively large specific surface, pore volume and porous distribution, which can absorb PS in the nanopores of Azo-COF effectively. Even the performance can hardly compare to those traditional carbon-based hosts with large specific surface area and pore volume,[10, 14] still a great progress in the hosts based on COFs.[32, 33]

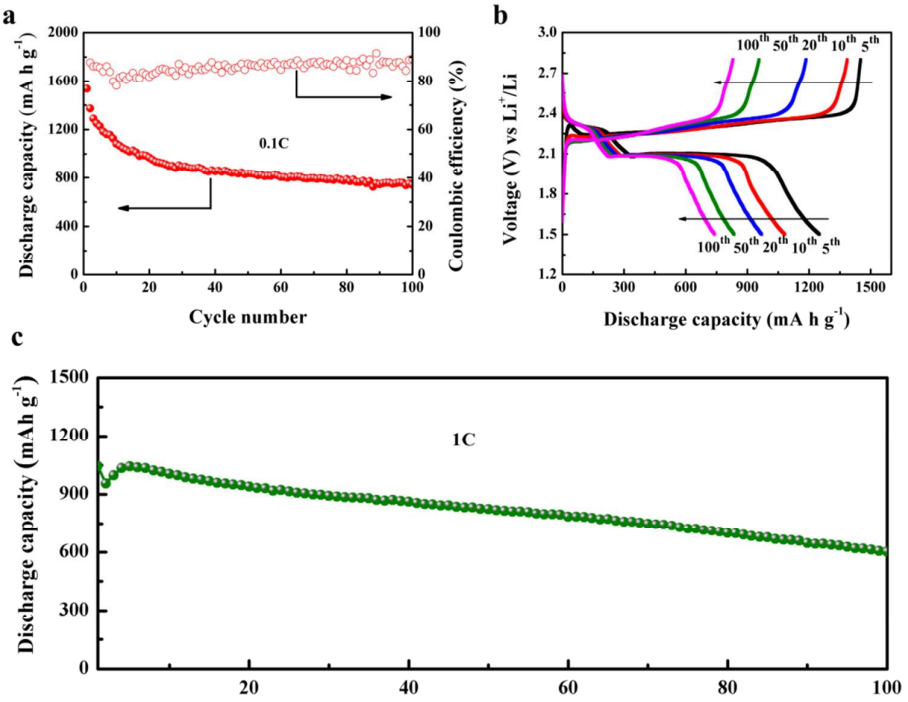

Fig. 6 Electrochemical properties of the S/Azo-COF electrodes. (a) Cycling performance of S/Azo-COF electrode at 0.1 C. (b) Discharge/charge curves of S/Azo-COF electrode at different cycles at 0.1 C. (c) Cycling performance of S/Azo-COF electrode at a high rate of 1 C.

Journal Name

ARTICLE

The C-rate behavior of the S/Azo-COF was evaluated via galvanostatic charge–discharge at different C-rates ranging from 0.1 to 2 C. As shown in Fig. 7a, with increasing the C-rate, the discharge capacity decreased gradually, which can be mainly attributed to polarization effect. For example, when the C-rate increased to 2 C from 0.1 C, the potential between the charge plateau and the second discharge plateau increased sharply from 148 to 547 mV, which is harmful for capacity output (Fig. 7c). Even so, a high rate capacity of 770 mA h g^{-1} was remained at a C-rate of 2 C (Fig. 7b), further suggesting the excellent rate performance.

In order to further understand the relationship between electrochemical performance and Azo-COF's pore distribution, two parameters of U_1 and Q_2/Q_1 were introduced. U_1, the onset potential of the plateau around 2.3 V, can reflect the interfacial kinetics between carbon and sulfur. Q_1 and Q_2 represent the partial discharge capacity of Q_0, the theoretical specific capacity of 1675 mA h g^{-1}, at the plateau around 2.3 V and 2.1 V as follows (Fig. 7d):

Plateau around 2.3 V:

$$S_8 + 4e^- \longleftrightarrow 2S_4^{2-}$$

$$Q_1 = 1/4Q_0,\ Q_0 = 1672\ mA\,h\,g^{-1};$$

Plateau around 2.1 V:

$$2S_4^{2-} + (12 - 2n)e^- + (16 - 2n)Li^+ \longleftrightarrow nLi_2S_2 + (8 - 2n)Li_2S$$

$$Q_2 = (3/4 - n/8)Q_0,\ 0 \le n \le 4,\ 1 \le Q_2/Q_1 \le 3.$$

The plateau around 2.3 V corresponds to transforming sulfur to soluble PS. Due to 1/2 electron per S transferring, a 1/4 of the theoretic capacity will be output at this plateau. The other one around 2.1 V can be ascribed to further reducing PS to final products of Li_2S, during which the insoluble Li_2S_2 and Li_2S species will precipitate on the surface of lithium anode and greatly increase the resistance of Li^+/e^- transportation. Hence, Q_2/Q_1 should be a good indicator to show the ability of Li^+/e^- transport within the host.[46,47] Fig. 7e and f show the evolutions of U_1 and Q_2/Q_1 for S/Azo-COF electrode with the increase of C-rate. It should be mentioned that the data were collected from the charge/discharge profiles at different C-rates of S/Azo-COF, as shown in Fig. 7c. As can be clearly seen, with increasing the C-rate, both U_1 and Q_2/Q_1 show a trend to decrease, which can be mainly attributed to the growing impedance of both ohmic resistance and charge-transfer resistance. Nevertheless, U_1 and Q_2/Q_1 of S/Azo-COF electrode still were maintained at 2.23 V and 1.73 at a high C-rate of 2 C, respectively, suggesting the relative superior reaction kinetics and fast Li^+/e^- transport for S/Azo-COF electrodes, which agrees well with the C-rate performance. Therefore, these results further highlighted the merit of Azo-COF host in facilitating electrolyte immersion and diffusion with a 1D regular pore distribution at 2.6 nm.

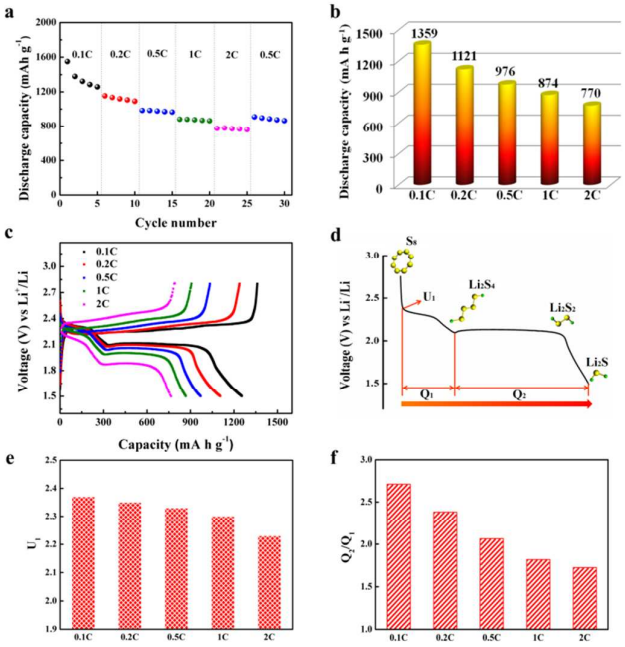

Fig. 7 Electrochemical properties of the S/Azo-COF electrode. (a) and (b) C-rate performance for S/Azo-COF electrode at various C-rates from 0.1 to 2 C. (c) Charge/discharge profiles for S/Azo-COF at various C-rates from 0.1 to 2 C. (d) Schematic illustration of a typical voltage profile. (e) and (f) The dependence of U_1 and Q_2/Q_1 on the C- rate (data are collected from Fig. 7c).

Conclusion

In summary, we have prepared the Azo-COF with relatively large specific surface area, pore volume and regular pore distribution as a promising sulfur host for Li-S batteries. The small mesopores distributed at 2.6 nm can limit the PS diffusion while providing attractive 1D channels for facilitating Li^+ transportation. On the basis of this intention, not only a high stable capacity of 741 mA h g^{-1} was remained after 100 cycles at 0.1 C but also a high rate capacity of 770 mA h g^{-1} at 2 C were achieved. Even the performance is not comparable to that of some carbon-based host systems, this research still presents the potential to arouse significant interest to the further development of Li-S batteries, and even such other electrochemical devices as capacitors and Li-O_2 batteries.

Acknowledgements

The authors acknowledge the National Natural Science Foundation of China (Grant No. 21406221, 21273235 and 51403209), and 100 Talents Program of Dalian Institute of Chemical Physics, Chinese Academy of Sciences.

Notes and references

1. A. Manthiram, Y. Fu, S. H. Chung, C. Zu and Y. S. Su, *Chem. Rev.*, 2014, **114**, 11751-11787.
2. S. Zhang, K. Ueno, K. Dokko and M. Watanabe, *Adv. Energy Mater.*, 2015, 1500212 | DOI: 10.1002/aenm.201500117.
3. X. Ji, K. T. Lee and L. F. Nazar, *Nat. Mater.*, 2009, **8**, 500-506.
4. A. Rosenman, E. Markevich, G. Salitra, D. Aurbach, A. Garsuch and F. F. Chesneau, *Adv. Energy. Mater.*, 2015, 1500212 |DOI: 10.1002/aenm. 201500212.
5. X. Ji and L. F. Nazar, *J. Mater. Chem.*, 2010, **20**, 9821-9826.
6. B. Zhang, X. Qin, G. R. Li and X. P. Gao, *Energy Environ. Sci.*, 2010, **3**, 1531-1537.
7. L. Sun, M. Li, Y. Jiang, W. Kong, K. Jiang, J. Wang and S. Fan, *Nano Lett.*, 2014, **14**, 4044-4049.
8. P. G. Bruce, S. A. Freunberger, L. J. Hardwick and J.-M. Tarascon, *Nat. Mater.*, 2011, **11**, 19-29.
9. S. Moon, Y. H. Jung, W. K. Jung, D. S. Jung, J. W. Choi and D. K. Kim, *Adv. Mater.*, 2013, **25**, 6547-6553.
10. Y. Zhao, W. Wu, J. Li, Z. Xu and L. Guan, *Adv. Mater.*, 2014, **26**, 5113-5118.
11. J. T. Lee, Y. Zhao, S. Thieme, H. Kim, M. Oschatz, L. Borchardt, A. Magasinski, W. I. Cho, S. Kaskel and G. Yushin, *Adv. Mater.*, 2013, **25**, 4573-4579.
12. N. Brun, K. Sakaushi, L. Yu, L. Giebeler, J. Eckert and M. M. Titirici, *Phys. Chem. Chem. Phys.*, 2013, **15**, 6080-6087.
13. L. Yu, N. Brun, K. Sakaushi, J. Eckert and M. M. Titirici, *Carbon*, 2013, **61**, 245-253.
14. M. Wang, H. Zhang, Q. Wang, C. Qu, X. Li and H. Zhang, *ACS Appl. Mater. Interfaces*, 2015, **7**, 3590-3599.
15. C. Liang, N. J. Dudney and J. Y. Howe, *Chem. Mater.*, 2009, **21**, 4724-4730.
16. S. Xin, L. Gu, N. H. Zhao, Y. X. Yin, L. J. Zhou, Y. G. Guo and L. J. Wan, *J. Am. Chem. Soc.*, 2012, **134**, 18510-18513.
17. Q. Li, Z. Zhang, Z. Guo, Y. Lai, K. Zhang and J. Li, *Carbon*, 2014, **78**, 1-9.
18. M. Rao, X. Geng, X. Li, S. Hu and W. Li, *J. Power Sources*, 2012, **212**, 179-185.
19. D. Lee, J.-Y. Jung, M.-J. Jung and Y.-S. Lee, *Chem. Eng. J.*, 2015, **263**, 62-70.
20. R. Singhal, S. Chung, A.Manthiram and V. Kalra, *J. Mater. Chem. A*, 2015, **3**, 4530-4538.
21. Z. Wang, Y. Dong, H. Li, Z. Zhao, H. B. Wu, C. Hao, S. Liu, J. Qiu and X. W. Lou, *Nat. Commun.*, 2014, **5**, 5002| DOI: 10.1038/ncomms6002.
22. G. Zhou, S. Pei, L. Li, D.-W. Wang, S. Wang, K. Huang, L.-C. Yin, F. Li and H.-M. Cheng, *Adv. Mater.*, 2014, **26**, 625-631.
23. H. Wang, Y. Yang, Y. Liang, J. T. Robinson, Y. Li, A. Jackson, Y. Cui and H. Dai, *Nano Lett.*, 2011, **11**, 2644-2647.
24. S. Yuan, Z. Guo, L. Wang, S. Hu, Y. Wang and Y. Xia, *Adv. Sci.*, 2015, 1500071| DOI: 10.1002/advs.201500071.
25. M. Xiao, M. Huang, S. Zeng, D. Han, S. Wang, L. Sun and Y. Meng, *RSC Adv.*, 2013, **3**, 4914-4916.
26. Y. Dong, S. Liu, Z. Wang, Y. Liu, Z. Zhao and J. Qiu, *Nanoscale*, 2015, **7**, 7569-7573.
27. X. Liang, Y. Liu, Z. Wen, L. Huang, X. Wang and H. Zhang, *J. Power Sources*, 2011, **196**, 6951-6955.
28. N. Nakamura, T. Yokoshima, H. Nara, T. Momma and T. Osaka, *J. Power Sources*, 2015, **274**, 1263-1266.
29. W. Zhou, Y. Yu, H. Chen, F. J. DiSalvo and H. D. Abruna, *J. Am. Chem. Soc.*, 2013, **135**, 16736-16743.
30. Z. Wei Seh, W. Li, J. J. Cha, G. Zheng, Y. Yang, M. T. McDowell, P. C. Hsu and Y. Cui, *Nat. Commun.*, 2013, **4**, 1331 | DOI: 10.1038/ ncomms2327.
31. X. Liang, C. Hart, Q. Pang, A. Garsuch, T. Weiss and L. F. Nazar, *Nat. Commun.*, 2015, **6**, 5682 | DOI: 10.1038/ncomms6682..
32. B. Guo, T. Ben, Z. Bi, G. M. Veith, X. G. Sun, S. Qiu and S. Dai, *Chem. Commun*, 2013, **49**, 4905-4907.
33. H. Liao, H. Ding, B. Li, X. Ai and C. Wang, *J. Mater. Chem. A*, 2014, **2**, 8854-8858.
34. S. Chandra, T. Kundu, S. Kandambeth, R. BabaRao, Y. Marathe, S. M. Kunjir and R. Banerjee, *J. Am. Chem. Soc.*, 2014, 136, 6570-6573.
35. R. Elazari, G. Salitra, A. Garsuch, A. Panchenko and D. Aurbach, *Adv. Mater.*, 2011, **23**, 5641-5644.
36. C. Zhang, H. Wu, C. Yuan, Z. Guo and X. D. Lou, *Angew. Chem. Int. Ed.*, 2012, **51**, 9592 –9595.
37. L. Miao, W. Wang, A. Wang, K. Yuan and Y. Yang, *J. Mater. Chem. A*, 2013, **1**, 11659-11664.
38. M. Wang, Y. Zhang, H. Zhang and H. Zhang, *ChemPlusChem*, 2014, **79**, 919-924.
39. Z. Yang, H. Wang, X. Zhong, W. Qi, B. Wang and Q. Jiang, *RSC Adv.*, 2014, **4**, 50964-50968.
40. X. Yang, N. Yan, W. Zhou, H. Zhang, X. Li and H. Zhang, *J. Mater. Chem. A,* 2015, **3**, 15314-15323..
41. Z. Li, Y. Jiang, L. Yuan, Z.Yi, C. Wu, Y. Liu, P. Strasser and Y. Huang, *ACS nano*, 2014, **8**, 9295-9303.
42. Z. Yang, H. Wang, X. Zhong, W. Qi, B. Wang and Q. Jiang, *RSC Adv.*, 2014, **4**, 50964–50968.
43. I. Y. Choi, H. Kim and M. J.Park, *RSC Adv.*, 2014, **4**, 61333–61336.
44. G. Zheng, Y. Yang, J. J. Cha, S. S. Hong and Y. Cui, *Nano Lett.*, 2011, **11**, 4462-4467.
45. C. Tang, Q. Zhang, M. Q. Zhao, J. Q. Huang, X. B. Cheng, G. L. Tian, H. J. Peng and F. Wei, *Adv. Mater.*, 2014, **26**, 6100-6105.
46. J. Zhou, R. Li, X. Fan, Y. Chen, R. Han, W. Li, J. Zheng, B. Wang and X. Li, *Energy Environ. Sci.*, 2014, **7**, 2715-2724.
47. M.-S. Park, J.-S. Yu, K. J. Kim, G. Jeong, J.-H. Kim, Y.-N. Jo,U. Hwang, S. Kang, T. Woo and Y.-J. Kim, Phys. Chem. Chem. Phys., 2012, **14**, 6796-6804.